L2A+

Enhanced Aeolus L2A for depolarizing targets and impact on aerosol research and NWP

-

"ASKOS ground-based datasets in support of L2A+"
Deliverable Item 02
[DI02]
(Final Version - FV)

Submitted to: Edward Malina (ESA)

	Name	Function	Date
Prepared by:	A. A. Floutsi	WP2000 – TROPOS	08/2024
	H. Baars	WP2000 – Co-I – TROPOS	08/2024
	E. Proestakis	WP1000 - NOA	08/2024
Approved by:	V. Amiridis	PI	08/2024

-

National Observatory of Athens (NOA)
Institute for Astronomy, Astrophysics, Space Applications & Remote Sensing (IAASARS)
Vas. Pavlou & I. Metaxa, 15236 Penteli, Greece
&
Leibniz Institute for Tropospheric Research (TROPOS), Leipzig, Germany
&
European Centre for Medium-Range Weather Forecasts
[ECMWF]
Reading, United Kingdom

[This page is intentionally left blank.]

Table of Contents

1. ESA-L2A+ DI02 – Overview

This document consists the final version (FV) of the Deliverable Item 02 (DI02) – Version 4 (V4.1) submitted to the European Space Agency (ESA) by the consortium of the project "Enhanced Aeolus L2A for depolarizing targets and impact on aerosol research and NWP" (L2A+).
The overall objective of WP2000 in L2A+ is to provide datasets of ground-based measurements conducted during the ASKOS campaign in Mindelo, Cabo Verde for the L2A+ product validation and model evaluation studies. In particular, a unique feature mask over Mindelo (D2) was created specifically for this purpose, based on the Cloudnet and EARLINET lidar target categorization. Aerosol optical properties, wind speed (Mindelo), and radiosonde profiles obtained at Sal were also considered for the ASKOS measurement periods. Height-resolved dust properties are of high relevance for L2A+ and, therefore, POLIPHON (Mamouri and Ansmann 2014, 2016) was applied to the ground-based PollyXT lidar data to retrieve the estimation of the vertically-resolved dust fraction above Mindelo (D5).
In accordance with WP2000 the present DI was initially submitted at KO+6 and updated at KO+15 and finalized at KO+21 months, respectively.

2. Introduction

In June 2021, within the framework of the ASKOS/JATAC campaign at Mindelo, Cabo Verde (2021-2022), TROPOS deployed a ground-based, multiwavelength-Raman-polarization lidar PollyXT, a HALO wind lidar, a CIMEL sun-photometer, and an RPG microwave radiometer. All instruments were continuously measuring during all the ASKOS intensive measurement periods (September 2021, June, and September 2022).
All PollyXT lidar measurements and products have been publicly available in near-real-time via polly.tropos.de (last access: 22 August 2024). Additionally, all ASKOS datasets, including the PollyXT lidar measurements, are hosted in NOA's ASKOS server and in the ESA Atmospheric Validation Data Centre (EVDC; Amiridis et al., 2023, last access: 22 August 2024).
In addition, an EarthCARE-like aerosol typing algorithm, HETEAC- Flex (Floutsi et al., 2024), was applied to selected measurements from the ground-based lidar in Mindelo to retrieve the mixing ratio (in terms of relative volume) of four aerosol components (representing the most abundant aerosol types in nature), along with the volume concentration of mineral dust (described in detail in Section 6).
Table 1 summarizes the different datasets provided within WP2000, along with their sources, formats, availabilities and versions. In addition, tables with the complete variable list, dimensions and units for the most important WP2000 datasets is provided in the Appendix. Currently, the dataset of WP2000 is hosted by NOA and the credential information can be found in Section 7.

Table 1: Products delivered in the framework of L2A+ WP2000.

Products	Instrument / Source	Format	Availability	Version
PollyXT Target classification	PollyXT Lidar	.nc file	September 2021, 2022 June 2022	V2
PollyXT Target classification V2	PollyXT Lidar	.nc file	September 2021, 2022 June 2022	V2
PollyXT profiles	PollyXT Lidar	.nc file	September 2021, 2022 June 2022	V2
POLIPHON	PollyXT Lidar	.nc file	September 2021, 2022 June 2022	V2
HETEAC-Flex	PollyXT Lidar	.txt file	03, 10, 17, 24 September 2021	V1

Feature mask	PollyXT Lidar	.nc file	September 2021, 2022 June 2022	V1
Meteorological variables	Radiosonde	.txt file	September 2021	V1

3. Data set of time series of height-resolved feature mask over Mindelo for September 2021 including aerosol optical properties

A comprehensive overview of the PollyXT lidar measurements conducted during the ASKOS intensive measurement periods is shown in Fig. 1. The attenuated backscatter coefficient at 1064 nm (Fig. 1a, 1c, 1e) in combination with the volume depolarization ratio at 532 nm (Fig. 1b, 1d, 1f) reveal that the typical aerosol conditions above Mindelo are a clean marine boundary layer (MBL; non-depolarizing spherical particles), with a dust aerosol layer (depolarizing non-spherical particles) on top of that.
For the ASKOS intensive measurement months, a total number of 1469 cloud-free profiles of aerosol optical properties were derived and delivered for L2A+, as part of D2. Among others, the vertically-resolved aerosol extinction and backscatter coefficient, lidar ratio and particle linear depolarization ratio are provided (detailed description is given in the Appendix).

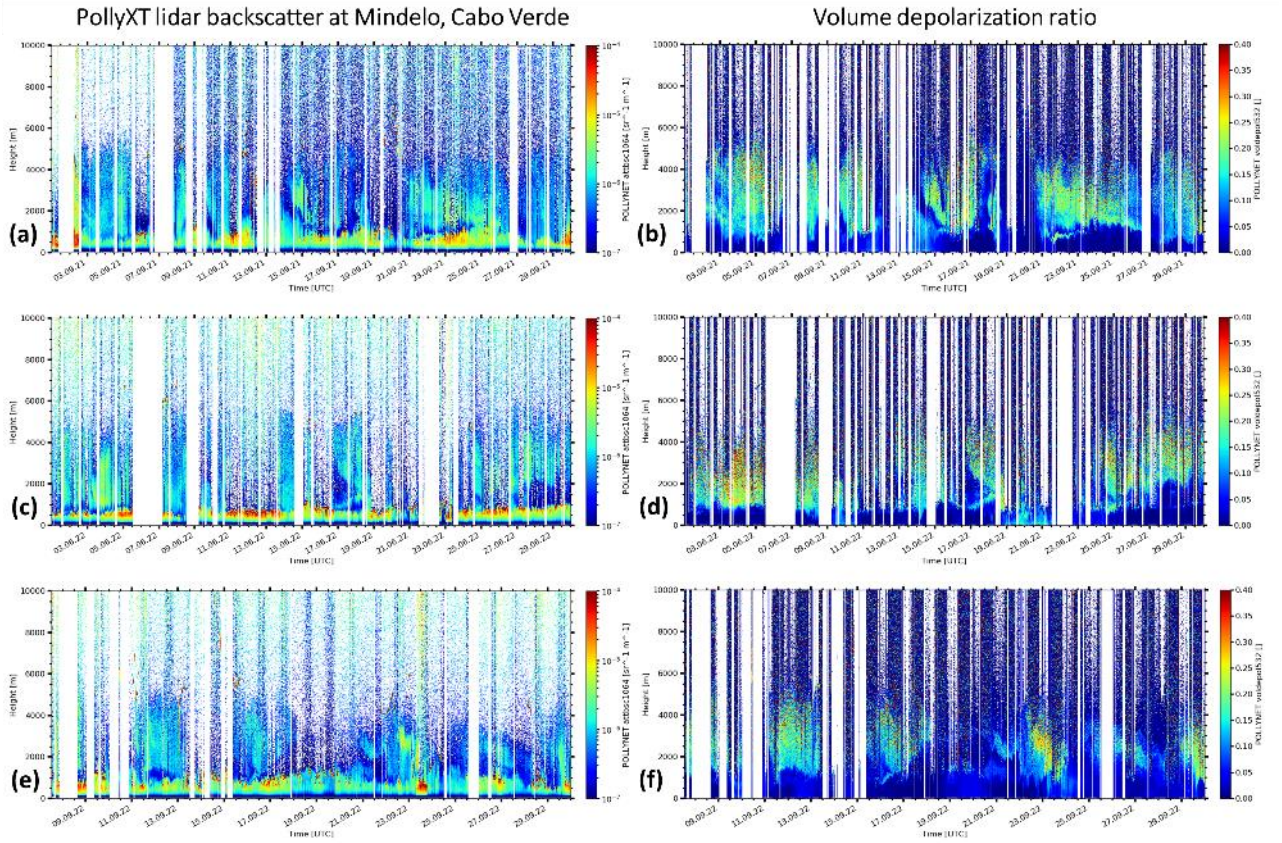

Figure 1: Overview of the lidar attenuated backscatter coefficient at 1064 nm (left column) and volume depolarization ratio at 532 nm (right column) as retrieved from the PollyXT lidar during the ASKOS operations in September 2021 (a, b), June 2022 (c, d), and September 2022 (e, f).

At Mindelo, cloud formation is very frequent at the top of the marine boundary layer (around 2 km) and at the top of the dust layer (e.g., around 5.5 km or above 6 km). It is therefore crucial to ensure that the derived profiles of aerosol optical properties are being properly screened for clouds. Apart

from the automatic routines in place (within the PollyNet processing chain; Yin & Baars, 2021), a manual inspection was performed to the ASKOS data. From a total of 2771 profiles, only 1469 were found to be totally or mostly cloud-free. The cloud- contaminated profiles have been therefore discarded and are not considered further for this study.

Within WP2000, an attempt to improve the respective cloud-screening routines was performed, before the final data delivery. However, the stricter criteria (threshold values of the backscatter coefficient) in many cases filtered out also useful data, most notably, intense dust events. Due to the decreased number of available profiles, as well as the decreased confidence in the screening criteria, this reprocessed version of the dataset was not delivered. A more sophisticated cloud-screening procedure, which utilizes the target classification is currently being developed (not associated with any deliverable within WP2000).

Based on a synergistic use of the lidar and radar in Mindelo, a novel cloud and feature mask has been created, especially for the L2A+ project. To achieve this, the EARLINET automatic target categorization based on lidar data (Baars et al., 2017) is being used in combination with the Cloudnet classification (CLU 2023) retrieved in synergistic use with ESAs cloud radar. The final product, which is the combined target classification, utilizes the aerosol classification based on the lidar data and the cloud classification from radar in a common grid. An example of this new feature mask is provided in Fig. 2. On this day (15 September 2021), we see that the MBL consists mainly of large, spherical aerosol (marine) with significant anthropogenic contributions (small aerosol) from around 06:00 to 20:00 UTC. After 20:00 UTC, liquid droplet clouds started to form. Above the MBL, between 2 and 4 km, a mineral dust aerosol layer was present. At around 12 km, a cirrus cloud was observed.
The Cloudnet target classification is one of the highest-level products, i.e., it requires several information from multiple instruments. Therefore, the creation of this target classification failed relatively often (mainly due to technical problems with the cloud radar). This was the case for several days within the ASKOS intensive measurement periods, resulting in an availability of the combined target classification mask for a total of 55 days only.

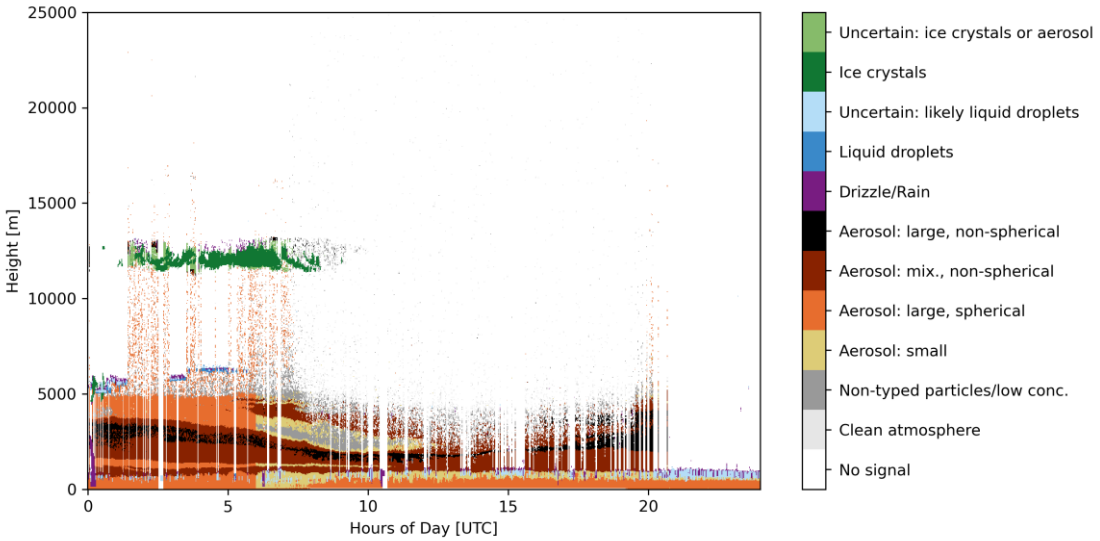

Figure 2: Combined target classification from lidar and radar synergy for 15 September 2021 at Mindelo, Cabo Verde.

4. Documentation on time series of profiles of wind speed over Mindelo and radiosonde profiles obtained at Sal

Wind speed and direction

Doppler wind lidar measurements were acquired continuously during all the ASKOS intensive measurement periods. An overview of the wind speed (a, c, e) and direction (b, d, f) for the months of September 2021 (top row), June 2022 (middle row) and September 2022 (bottom row) is shown in Fig. 3. Horizontal wind can be derived in the PBL and in the SAL in case of sufficient backscatter signal. In cases of low aerosol load (e.g., on the 20 September 2021), no winds can be derived above the PBL.

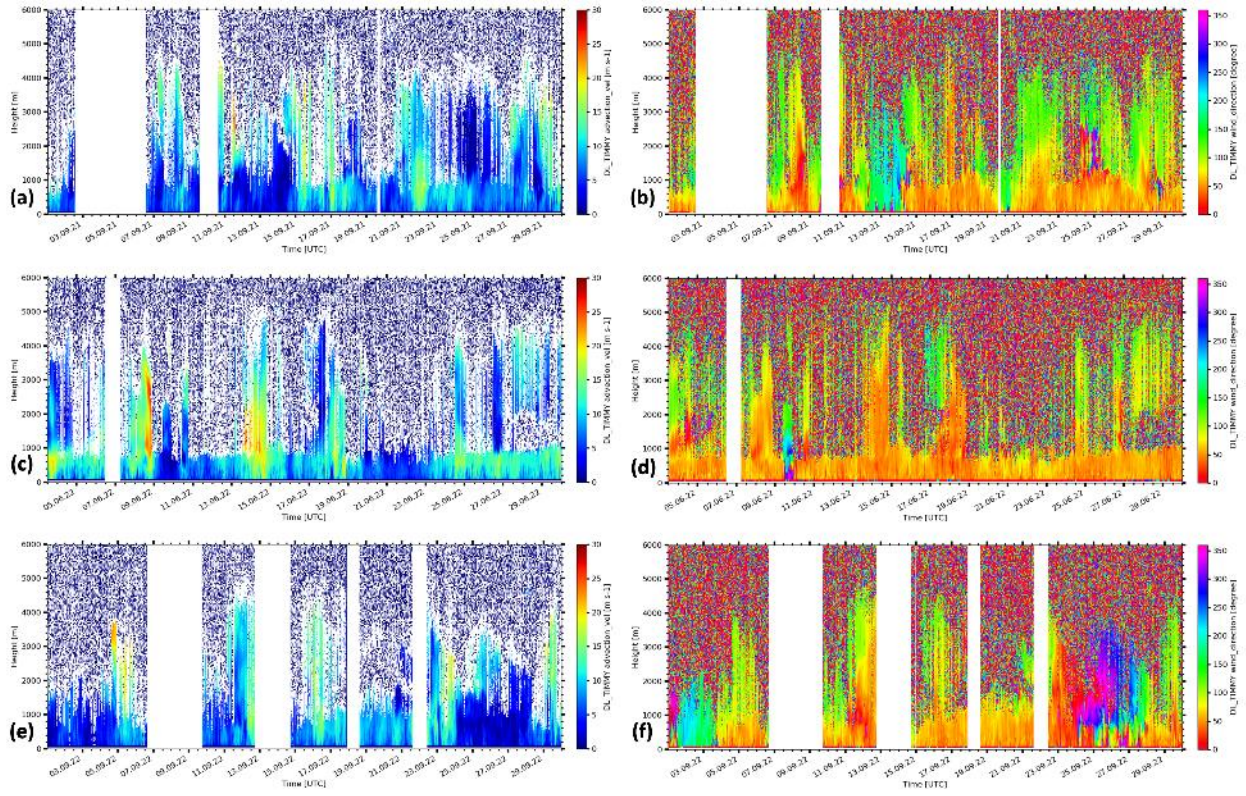

Figure 3: Overview of the Doppler wind lidar derived wind speed (left) and direction (right) during the ASKOS operations in September 2021 (a, b), June 2022 (c, d), September 2022 (e, f).

Radiosonde profiles at Sal

Radiosondes releases (Borne et al., 2023) were performed daily at Sal airport, Sal, Cabo Verde between 07 and 28 September 2021. A total number of 37 releases were performed during that time. The radiosonde schedule, which was designed to align the radiosonde releases and the Aeolus overpasses, is summarized in Table 3. The releases were performed with the iMet-4 radiosondes from the International Met System and provided measurements of wind speed, wind direction, temperature, humidity, and air pressure.

Table 2: Weekly schedule of the radiosonde releases at Sal.

Weekday	Radiosonde release time [UTC]
Monday	06:40, 10:45
Tuesday	06:50, 10:45
Wednesday	07:00, 10:45
Thursday	18:50, 10:45
Friday	19:00, 10:45
Saturday	10:45
Sunday	10:45

5. Vertically-resolved dust profiles

POLIPHON is a powerful tool that among others, can be used for the separation of dust and non-dust aerosol by combining the unique capabilities of the polarisation lidar with the well-established global aerosol optical and microphysical climatologies of AERONET. The POLIPHON (Mamouri and Ansmann 2014, 2016) analysis comprises two steps. The first step is the analysis of the polarisation lidar observations based on the different polarisation properties of the different aerosol types to obtain vertically-resolved profiles of dust and non-dust backscatter coefficients, and thus the backscatter-related dust fraction. Then, by means of the appropriate dust extinction-to-backscatter ratios (lidar ratios), the dust and non-dust backscatter coefficients are converted to the respective dust and non-dust extinction coefficients. The second step of the analysis is the derivation of the vertically-resolved profile of the dust mass concentration (for both fine and coarse dust particles) from the respective extinction coefficients by utilising extinction-to-volume conversion factors that were determined from AERONET observations. Further products that can be derived with the POLIPHON method include the particle number, surface area, and volume concentration for dust and non-dust aerosol components as well as CCN and INP concentrations. For the purposes of L2A+, the two step POLIPHON analysis was performed.

The input for the first step POLIPHON, are the PollyNET profiles of backscatter, extinction and particle linear depolarization ratio at all available wavelengths. The output are vertically resolved profiles of dust and non-dust backscatter and extinction coefficients, as demonstrated in Fig. 4 for the 532-nm backscatter coefficient on 10 September 2021 between 19:00 and 19:56 UTC (within the Aeolus overpass).

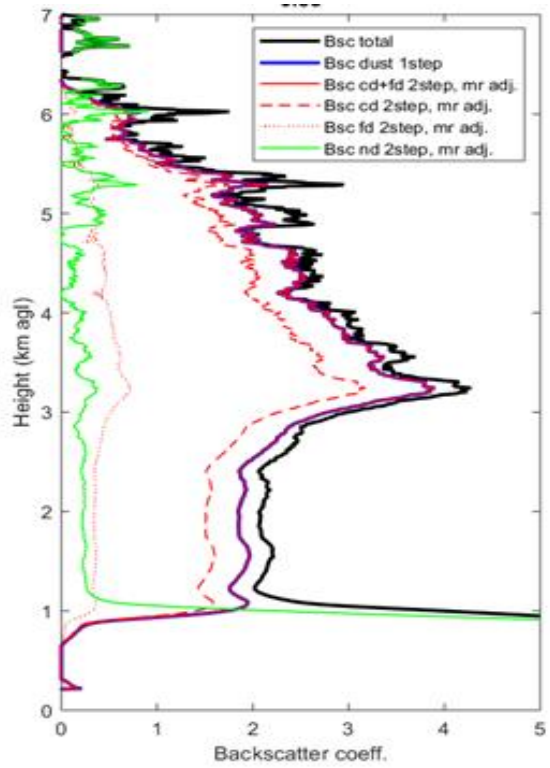

Figure 4: Dust (blue and red lines) and non-dust (green) contribution in terms of backscatter coefficient (PollyXT) as derived using the two-step POLIPHON methodology for Mindelo on 10 September 2021 between 19:00 and 19:56 UTC. On the second step, the dust contribution is further separated into coarse and fine mode (red dashed and dotted line, respectively).

6. HETEAC-Flex

HETEAC-Flex is an aerosol typing scheme based on the optimal estimation method applicable to both ground-based and spaceborne lidars (Floutsi et al., 2024). HETEAC-Flex is an EarthCARE-like algorithm that it is consistent with HETEAC (Hybrid End-To-End Aerosol Classification), an aerosol classification model that was developed for the EarthCARE mission (Wandinger et al., 2023).

HETEAC-Flex can be applied to retrieve the relative volume contribution of four different aerosol components, which comprise two fine (absorbing and non-absorbing) and two coarse modes (spherical and non-spherical). The aerosol components represent the most common aerosol types observed in nature, i.e., smoke, pollution, marine and desert dust, respectively. The HETEAC-Flex results can be used to calculate additional products, including the number and volume concentration per aerosol component as well as the refractive index and effective radius of the mixture.

Within this DI (DI02), HETEAC- Flex has been applied for the four Friday Aeolus overpasses of September 2021 (03, 10, 17 and 24). An example is shown in Fig. 5. Both, HETEAC-Flex and POLIPHON are consistent in identifying the dominance of desert dust in the aerosol layer. The non-dust POLIPHON contributions can be quantitatively attributed to three aerosol components with HETEAC- Flex.

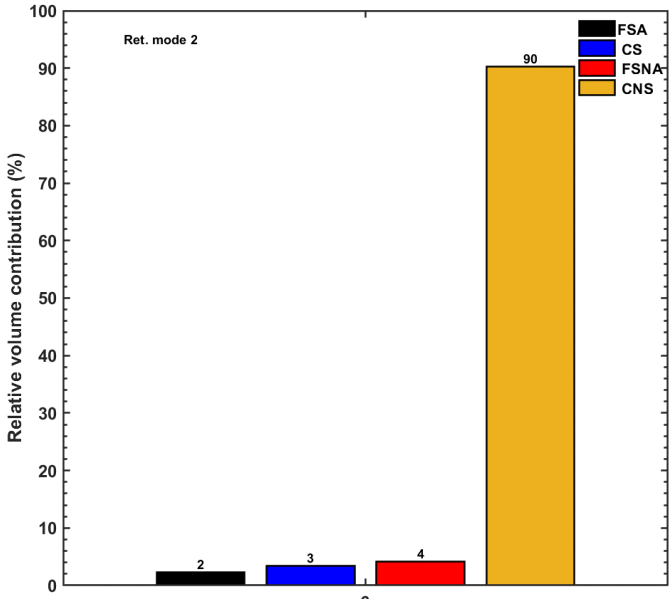

Figure 5: HETEAC-Flex results for the aerosol layer observed between 2.5 and 4 km above Mindelo on 10 September 2021 between 19:00 and 19:56 UTC. The relative volume contribution for Coarse Spherical (CS), Coarse Non-Spherical (CNS), Fine absorbing (FA) and fine none absorbing (FNA) is presented.

7. Access Credentials

Access to the ESA-L2A+ products are provided according to the following access credentials:

Table 6: ESA-L2A+ WP2000 access credentials.

L2A+ OPs	
Protocol:	SFTP (Port 22)
Username:	l2aplus_wp2000
Password:	eYst5kuxngzn
Host:	react.space.noa.gr

8. Contact Person(s)

Contact:

Users can contact with Athena Floutsi (floutsi@tropos.de) and/or Holger Baars (baars@tropos.de) for any further details and clarifications regarding the L2A+ dataset. For tackling server issues in accessing NOA servers users can contact with Thanasis Georgiou (ageorgiou@noa.gr).

Acronyms and Abbreviations

JATAC	Joint Aeolus Tropical Atlantic Campaign
POLIPHON	Polarisation Lidar Photometer Networking
AERONET	Aerosol Robotic Network
HETEAC	Hybrid End-To-End Aerosol Classification

List of Figures

List of Tables

References

Amiridis, V., Eleni, M., Peristera, P., Holger, B., Razvan, P., Engelmann, R., Alexandra, T., Ioanna, T., Vasiliki, D., Stelios, K., Skupin, A., Franco, M., Maria, K., Dimitra, K., Nikolaos, S., Floutsi, A. A., Spiros, M., Vasileios, S. M., Panagiotis, R., Althausen, D., Seifert, P., Nemuc, A., Antonescu, B., Alkistis, P., and Wandinger, U.: ASKOS Campaign Dataset, https://doi.org/10.60621/jatac.campaign.2021.2022.caboverde, 2023.

Baars, H., Seifert, P., Engelmann, R., and Wandinger, U.: Target categorization of aerosol and clouds by continuous multiwavelength-polarization lidar measurements, Atmos. Meas. Tech., 10, 3175–3201, https://doi.org/10.5194/amt-10-3175-2017, 2017.

Borne, M., Knippertz, P., Weissmann, M., Witschas, B., Flamant, C., Rios-Berrios, R., and Veals, P.: Validation of Aeolus L2B products over the tropical Atlantic using radiosondes, Atmos. Meas. Tech., 17, 561–581, https://doi.org/10.5194/amt-17-561-2024, 2024.

CLU (2023): Cloud profiling product: Classification; 2021-09-09 to 2021-09-30; from Mindelo. Generated by the cloud profiling unit of the ACTRIS Data Centre, https://hdl.handle.net/21.12132/2.bbd79a556daa477d, 2023.

Floutsi, A. A., Baars, H., and Wandinger, U.: HETEAC-Flex: an optimal estimation method for aerosol typing based on lidar-derived intensive optical properties, Atmos. Meas. Tech., 17, 693–714, https://doi.org/10.5194/amt-17-693-2024, 2024.

Mamouri, R. E. and Ansmann, A.: Fine and coarse dust separation with polarization lidar, Atmos. Meas. Tech., 7, 3717–3735, https://doi.org/10.5194/amt-7-3717-2014, 2014.

Mamouri, R.-E. and Ansmann, A.: Potential of polarization lidar to provide profiles of CCN- and INP-relevant aerosol parameters, Atmos. Chem. Phys., 16, 5905–5931, https://doi.org/10.5194/acp-16-5905-2016, 2016.

Wandinger, U., Floutsi, A. A., Baars, H., Haarig, M., Ansmann, A., Hünerbein, A., Docter, N., Donovan, D., van Zadelhoff, G.-J., Mason, S., and Cole, J.: HETEAC – the Hybrid End-To-End Aerosol Classification model for EarthCARE, Atmos. Meas. Tech., 16, 2485–2510, https://doi.org/10.5194/amt-16-2485-2023, 2023.

Yin, Z., & Baars, H. (2021). Pollynet/pollynet processing chain: Version 3.0 (Version v3.0). Zenodo. https://doi.org/10.5281/zenodo.5571289 (last access: 22 August 2024).

Appendix

The unique height-resolved feature mask utilizes multiwavelength-Raman-polarisation lidar, cloud radar and microwave radiometer data and allows for high-performance cloud and feature detection (Combined Cloudnet + EARLINET lidar target categorization).

The filenames follow the structure: “YYYYMMDD_regridded_data_for_mindelo.nc”

Group	*Subgroup*	*Variable*	*Units*	*Dimensions*	*Description*
FEATURE MASK	-	cloudnet_LWP	g/m²	time	Liquid water path
		cloudnet_radar_gas_attenuation	dB	time, height	Two-way radar attenuation due to atmospheric gases
		cloudnet_radar_liquid_attenuation	dB	time, height	Two-way radar attenuation due to liquid water
		cloudnet_radar_v	m/s	time, height	Doppler velocity
		cloudnet_radar_width	m/s	time, height	Spectral width
		cloudnet_radar_Z	dBZ	time, height	Radar reflectivity factor
		cloudnet_radar_Z_error	dB	time, height	Error in radar reflectivity factor

		cloudnet_target_classification	1	time, height	Target classification
		combined_target_classification	1	time, height	Novel feature mask
		height	m	height	Height above mean sea level
		model_pressure	Pa	time, height	Pressure
		model_temperature	K	time, height	Temperature
		polly_ang_532_1064	1	time, height	Quasi backscatter-related Ångström exponent at 532-1064 nm
		polly_att_bsc_1064	sr^{-1} m^{-1}	time, height	Attenuated backscatter at 1064 nm
		polly_att_bsc_532	sr^{-1} m^{-1}	time, height	Attenuated backscatter at 532 nm
		polly_bsc_1064	sr^{-1} m^{-1}	time, height	Quasi aerosol backscatter coefficients at 1064 nm
		polly_bsc_1064_quality_flag	1	time, height	QC information
		polly_bsc_532	sr^{-1} m^{-1}	time, height	Quasi aerosol backscatter coefficients at 532 nm
		polly_bsc_532_quality_flag	1	time, height	QC information
		polly_pardepol_532	1	time, height	quasi particle depolarization ratio at 532 nm
		polly_target_classification	1	time, height	EARLINET lidar classification
		polly_voldepol_532	1	time, height	Volume depolarization ratio at 532 nm
		polly_voldepol_532_quality_flag	1	time, height	QC information
		time	UTC	time	Hours of day

The dataset also includes vertically-resolved aerosol optical properties derived from the PollyXT ground-based, multiwavelength, Raman, polarization lidar measurements.

The filenames follow the structure:
“YYYY_MM_DD_weekday_CPV_HH_MM_SS_HHMM_HHMM_profiles.nc”

Group	***Subgroup***	***Variable***	***Units***	***Dimensions***	***Description***

PollyXT PROFILES	-	aerBsc_aeronet_1064	sr^{-1} m^{-1}	height	Aerosol backscatter coefficient at 1064 nm retrieved with constrained-AOD method
		aerBsc_aeronet_355	sr^{-1} m^{-1}	height	Aerosol backscatter coefficient at 355 nm retrieved with constrained-AOD method
		aerBsc_aeronet_532	sr^{-1} m^{-1}	height	Aerosol backscatter coefficient at 532 nm retrieved with constrained-AOD method
		aerBsc_klett_1064	sr^{-1} m^{-1}	height	Aerosol backscatter coefficient at 1064 nm retrieved with Klett method
		aerBsc_klett_355	sr^{-1} m^{-1}	Height	Aerosol backscatter coefficient at 355 nm retrieved with Klett method
		aerBsc_klett_532	sr^{-1} m^{-1}	Height	Aerosol backscatter coefficient at 532 nm retrieved with Klett method
		aerBsc_raman_1064	sr^{-1} m^{-1}	height	Aerosol backscatter coefficient at 1064 nm retrieved with Raman method
		aerBsc_raman_355	sr^{-1} m^{-1}	Height	Aerosol backscatter coefficient at 355 nm retrieved with Raman method
		aerBsc_raman_532	sr^{-1} m^{-1}	height	Aerosol backscatter coefficient at 532 nm retrieved with Raman method
		aerBsc_RR_1064	sr^{-1} m^{-1}	height	Aerosol backscatter coefficient at 1064 nm retrieved with rotation Raman method
		aerBsc_RR_355	sr^{-1} m^{-1}	height	Aerosol backscatter

					coefficient at 355 nm retrieved with rotation Raman method
		aerBsc_RR_532	sr^{-1} m^{-1}	height	Aerosol backscatter coefficient at 532 nm retrieved with rotation Raman method
		aerExt_raman_1064	m^{-1}	height	Aerosol extinction coefficient at 1064 nm retrieved with Raman method
		aerExt_raman_355	m^{-1}	height	Aerosol extinction coefficient at 355 nm retrieved with Raman method
		aerExt_raman_532	m^{-1}	height	Aerosol extinction coefficient at 532 nm retrieved with Raman method
		aerExt_RR_1064	m^{-1}	height	Aerosol extinction coefficient at 1064 nm retrieved with rotation Raman method
		aerExt_RR_355	m^{-1}	height	Aerosol extinction coefficient at 355 nm retrieved with rotation Raman method
		aerExt_RR_532	m^{-1}	height	Aerosol extinction coefficient at 532 nm retrieved with rotation Raman method
		aerLR_raman_1064	sr	height	Aerosol lidar ratio at 1064 nm retrieved with Raman method
		aerLR_raman_355	sr	height	Aerosol lidar ratio at 355 nm retrieved with Raman method
		aerLR_raman_532	sr	height	Aerosol lidar ratio at 532 nm retrieved with Raman method
		aerLR_RR_1064	sr	height	Aerosol lidar ratio at 1064 nm retrieved with

					rotation Raman method
		aerLR_RR_355	sr	height	Aerosol lidar ratio at 355 nm retrieved with rotation Raman method
		aerLR_RR_532	sr	height	Aerosol lidar ratio at 532 nm retrieved with rotation Raman method
		altitude	m	1	Height of lidar above mean sea level
		end_time	seconds since 1970-01-01 00:00:00 UTC	1	Time UTC of the end of the current measurement
		height	m	height	Height above ground
		latitude	degrees north	1	Latitude of the site
		longitude	degrees east	1	Longitude of the site
		LR_aeronet_1064	sr	1	Aerosol lidar ratio at 1064 nm retrieved with constrained-AOD method
		LR_aeronet_355	sr	1	Aerosol lidar ratio at 355 nm retrieved with constrained-AOD method
		LR_aeronet_532	sr	1	Aerosol lidar ratio at 532 nm retrieved with constrained-AOD method
		parDepol_klett_1064	1	height	Particle linear depolarization ratio at 1064 nm with Klett backscatter
		parDepol_klett_355	1	height	Particle linear depolarization ratio at 355 nm with Klett backscatter
		parDepol_klett_532	1	height	Particle linear depolarization ratio at 532 nm with Klett backscatter

		parDepol_raman_1064	1	height	Particle linear depolarization ratio at 1064 nm with Raman backscatter
		parDepol_raman_355	1	height	Particle linear depolarization ratio at 355 nm with Raman backscatter
		parDepol_raman_532	1	height	Particle linear depolarization ratio at 532 nm with Raman backscatter
		pressure	hPa	height	Air pressure
		reference_height_1064	m	reference_height	Reference height for 1064 nm
		reference_height_355	m	reference_height	Reference height for 355 nm
		reference_height_532	m	reference_height	Reference height for 532 nm
		RH	%	height	Relative humidity
		shots	1	1	Accumulated laser shots
		start_time	seconds since 1970-01-01 00:00:00 UTC	1	Time UTC of the start of the current measurement
		temperature	degree Celsius	height	Air temperature
		uncertainty_aerBsc_aeronet_1064	$sr^{-1}\ m^{-1}$	height	Uncertainty of aerosol backscatter coefficient at 1064 nm
		uncertainty_aerBsc_aeronet_355	$sr^{-1}\ m^{-1}$	height	Uncertainty of aerosol backscatter coefficient at 355 nm
		uncertainty_aerBsc_aeronet_532	$sr^{-1}\ m^{-1}$	height	Uncertainty of aerosol backscatter coefficient at 532 nm
		uncertainty_aerBsc_klett_1064	$sr^{-1}\ m^{-1}$	height	Uncertainty of aerosol backscatter coefficient at 1064 nm
		uncertainty_aerBsc_klett_355	$sr^{-1}\ m^{-1}$	height	Uncertainty of aerosol backscatter

					coefficient at 355 nm
		uncertainty_aerBsc_klett_532	$sr^{-1}\ m^{-1}$	height	Uncertainty of aerosol backscatter coefficient at 532 nm
		uncertainty_aerBsc_raman_1064	$sr^{-1}\ m^{-1}$	height	Uncertainty of aerosol backscatter coefficient at 1064 nm
		uncertainty_aerBsc_raman_355	$sr^{-1}\ m^{-1}$	height	Uncertainty of aerosol backscatter coefficient at 355 nm
		uncertainty_aerBsc_raman_532	$sr^{-1}\ m^{-1}$	height	Uncertainty of aerosol backscatter coefficient at 532 nm
		uncertainty_aerBsc_RR_1064	$sr^{-1}\ m^{-1}$	height	Uncertainty of aerosol backscatter coefficient at 1064 nm
		uncertainty_aerBsc_RR_355	$sr^{-1}\ m^{-1}$	height	Uncertainty of aerosol backscatter coefficient at 355 nm
		uncertainty_aerBsc_RR_532	$sr^{-1}\ m^{-1}$	height	Uncertainty of aerosol backscatter coefficient at 532 nm
		uncertainty_aerExt_raman_1064	m^{-1}	height	Uncertainty of aerosol extinction coefficient at 1064 nm
		uncertainty_aerExt_raman_355	m^{-1}	height	Uncertainty of aerosol extinction coefficient at 355 nm
		uncertainty_aerExt_raman_532	m^{-1}	height	Uncertainty of aerosol extinction coefficient at 532 nm
		uncertainty_aerExt_RR_1064	m^{-1}	height	Uncertainty of aerosol extinction coefficient at 1064 nm
		uncertainty_aerExt_RR_355	m^{-1}	height	Uncertainty of aerosol extinction coefficient at 355 nm
		uncertainty_aerExt_RR_532	m^{-1}	height	Uncertainty of aerosol extinction

					coefficient at 532 nm
		uncertainty_aerLR_raman_1064	m^{-1}	height	Uncertainty of aerosol lidar ratio at 1064 nm
		uncertainty_aerLR_raman_355	sr	height	Uncertainty of aerosol lidar ratio at 355 nm
		uncertainty_aerLR_raman_532	sr	height	Uncertainty of aerosol lidar ratio at 532 nm
		uncertainty_aerLR_RR_1064	sr	height	Uncertainty of aerosol lidar ratio at 1064 nm
		uncertainty_aerLR_RR_355	sr	height	Uncertainty of aerosol lidar ratio at 355 nm
		uncertainty_aerLR_RR_532	sr	height	Uncertainty of aerosol lidar ratio at 532 nm
		uncertainty_parDepol_klett_1064	1	height	Uncertainty of particle linear depolarization ratio at 1064 nm with Klett backscatter
		uncertainty_parDepol_klett_355	1	height	Uncertainty of particle linear depolarization ratio at 355 nm with Klett backscatter
		uncertainty_parDepol_klett_532	1	height	Uncertainty of particle linear depolarization ratio at 532 nm with Klett backscatter
		uncertainty_parDepol_raman_1064	1	height	Uncertainty of particle linear depolarization ratio at 1064 nm with Raman backscatter
		uncertainty_parDepol_raman_355	1	height	Uncertainty of particle linear depolarization ratio at 355 nm with Raman backscatter
		uncertainty_parDepol_raman_532	1	height	Uncertainty of particle linear depolarization ratio at 532 nm with Raman backscatter
		uncertainty_volDepol_klett_1064	1	height	Uncertainty of volume

					depolarization ratio at 1064 nm
		uncertainty_volDepol_klett_355	1	height	Uncertainty of volume depolarization ratio at 355 nm
		uncertainty_volDepol_klett_532	1	height	Uncertainty of volume depolarization ratio at 532 nm
		uncertainty_volDepol_raman_1064	1	height	Uncertainty of volume depolarization ratio at 1064 nm
		uncertainty_volDepol_raman_355	1	height	Uncertainty of volume depolarization ratio at 355 nm
		uncertainty_volDepol_raman_532	1	height	Uncertainty of volume depolarization ratio at 532 nm
		uncertainty_WVMR	g/km	height	Absolute water vapor mixing ratio uncertainty
		volDepol_klett_1064	1	height	Volume linear depolarization ratio at 1064 nm with the same smoothing as Klett method
		volDepol_klett_355	1	height	Volume linear depolarization ratio at 355 nm with the same smoothing as Klett method
		volDepol_klett_532	1	height	Volume linear depolarization ratio at 532 nm with the same smoothing as Klett method
		volDepol_raman_1064	1	height	Volume linear depolarization ratio at 1064 nm with the same smoothing as Raman method
		volDepol_raman_355	1	height	Volume linear depolarization ratio at 355 nm with the same smoothing as Raman method
		volDepol_raman_532	1	height	Volume linear depolarization ratio at 532 nm with the same

					smoothing as Raman method
		WVMR	g/kg	height	Water vapor mixing ratio
		WVMR_no_QC	g/kg	height	Water vapor mixing ratio without quality control
		WVMR_rel_err	1	height	Relative error of the water vapor mixing ratio
		zenith_angle	degree	1	Zenith angle

The 1-step POLIPHON methodology was applied to the PollyXT ground-based lidar data to derive the height-resolved dust-only optical properties.

The filename follows the structure:

"YYYY_MM_DD_weekday_CPV_HH_MM_SS_HHMM_HHMM _POLIPHON_1.nc"

Group	*Subgroup*	*Variable*	*Units*	*Dimensions*	*Description*
DUST-ONLY (POLIPHON-1) PROFILES	-	aerBsc1064_klett_d1	sr^{-1} m^{-1}	height	One-step dust particle backscatter coefficient at 1064 nm retrieved with Klett method
		aerBsc1064_klett_nd1	sr^{-1} m^{-1}	height	One-step non-dust particle backscatter coefficient at 1064 nm retrieved with Klett method
		aerBsc1064_raman_d1	sr^{-1} m^{-1}	height	One-step dust particle backscatter coefficient at 1064 nm retrieved with Raman method
		aerBsc1064_raman_nd1	sr^{-1} m^{-1}	height	One-step non-dust particle backscatter coefficient at 1064 nm retrieved with Raman method
		aerBsc355_klett_d1	sr^{-1} m^{-1}	height	One-step dust particle backscatter

					coefficient at 355 nm retrieved with Klett method
		aerBsc355_klett_nd1	sr^{-1} m^{-1}	height	One-step non-dust particle backscatter coefficient at 355 nm retrieved with Klett method
		aerBsc355_raman_d1	sr^{-1} m^{-1}	height	One-step dust particle backscatter coefficient at 355 nm retrieved with Raman method
		aerBsc355_raman_nd1	sr^{-1} m^{-1}	height	One-step non-dust particle backscatter coefficient at 355 nm retrieved with Raman method
		aerBsc532_klett_d1	sr^{-1} m^{-1}	height	One-step dust particle backscatter coefficient at 532 nm retrieved with Klett method
		aerBsc532_klett_nd1	sr^{-1} m^{-1}	height	One-step non-dust particle backscatter coefficient at 532 nm retrieved with Klett method
		aerBsc532_raman_d1	sr^{-1} m^{-1}	height	One-step dust particle backscatter coefficient at 532 nm retrieved with Raman method
		aerBsc532_raman_nd1	sr^{-1} m^{-1}	height	One-step non-dust particle backscatter coefficient at 532 nm retrieved with Raman method
		aerBsc_klett_1064	sr^{-1} m^{-1}	height	Aerosol backscatter coefficient at 1064 nm

					retrieved with Klett method
		aerBsc_klett_355	sr^{-1} m^{-1}	height	Aerosol backscatter coefficient at 355 nm retrieved with Klett method
		aerBsc_klett_532	sr^{-1} m^{-1}	height	Aerosol backscatter coefficient at 532 nm retrieved with Klett method
		aerBsc_raman_1064	sr^{-1} m^{-1}	height	Aerosol backscatter coefficient at 1064 nm retrieved with Raman method
		aerBsc_raman_355	sr^{-1} m^{-1}	height	Aerosol backscatter coefficient at 355 nm retrieved with Raman method
		aerBsc_raman_532	sr^{-1} m^{-1}	height	Aerosol backscatter coefficient at 532 nm retrieved with Raman method
		altitude	m	1	Height of lidar above mean sea level
		end_time	seconds since 1970-01-01 00:00:00 UTC	1	Time UTC of the end of the current measurement
		height	m	height	Height above ground
		latitude	degrees north	1	Latitude of the site
		longitude	degrees east	1	Longitude of the site
		start_time	seconds since 1970-01-01 00:00:00 UTC	1	Time UTC of the start of the current measurement
		time	seconds since 1970-01-	time	Time

			01 00:00:00 UTC		
		uncertainty_aerBsc1064__nd1	sr^{-1} m^{-1}	height	Uncertainty of one-step non-dust particle backscatter coefficient at 1064 nm retrieved with Klett method
		uncertainty_aerBsc1064_klett_d1	sr^{-1} m^{-1}	height	Uncertainty of one-step dust particle backscatter coefficient at 1064 nm retrieved with Klett method
		uncertainty_aerBsc1064_raman_d1	sr^{-1} m^{-1}	height	Uncertainty of one-step dust particle backscatter coefficient at 1064 nm retrieved with Raman method
		uncertainty_aerBsc1064_raman_nd1	sr^{-1} m^{-1}	height	Uncertainty of one-step non-dust particle backscatter coefficient at 1064 nm retrieved with Raman method
		uncertainty_aerBsc355_klett_d1	sr^{-1} m^{-1}	height	Uncertainty of one-step dust particle backscatter coefficient at 355 nm retrieved with Klett method
		uncertainty_aerBsc355_klett_nd1	sr^{-1} m^{-1}	height	Uncertainty of one-step non-dust particle backscatter coefficient at 355 nm retrieved with Klett method
		uncertainty_aerBsc355_raman_d1	sr^{-1} m^{-1}	height	Uncertainty of one-step dust particle backscatter coefficient at 355 nm retrieved with Raman method

		uncertainty_aerBsc355_raman_nd1	sr^{-1} m^{-1}	height	Uncertainty of one-step non-dust particle backscatter coefficient at 355 nm retrieved with Raman method
		uncertainty_aerBsc532_klett_d1	sr^{-1} m^{-1}	height	Uncertainty of one-step dust particle backscatter coefficient at 532 nm retrieved with Klett method
		uncertainty_aerBsc532_klett_nd1	sr^{-1} m^{-1}	height	Uncertainty of one-step non-dust particle backscatter coefficient at 532 nm retrieved with Klett method
		uncertainty_aerBsc532_raman_d1	sr^{-1} m^{-1}	height	Uncertainty of one-step dust particle backscatter coefficient at 532 nm retrieved with Raman method
		uncertainty_aerBsc532_raman_nd1	sr^{-1} m^{-1}	height	Uncertainty of one-step non-dust particle backscatter coefficient at 532 nm retrieved with Raman method
		uncertainty_aerBsc_klett_1064	sr^{-1} m^{-1}	height	Uncertainty of aerosol backscatter coefficient at 1064 nm
		uncertainty_aerBsc_klett_355	sr^{-1} m^{-1}	height	Uncertainty of aerosol backscatter coefficient at 355 nm
		uncertainty_aerBsc_klett_532	sr^{-1} m^{-1}	height	Uncertainty of aerosol backscatter coefficient at 532 nm
		uncertainty_aerBsc_raman_1064	sr^{-1} m^{-1}	height	Uncertainty of aerosol backscatter

					coefficient at 1064 nm
		uncertainty_aerBsc_raman_355	sr^{-1} m^{-1}	height	Uncertainty of aerosol backscatter coefficient at 355 nm
		uncertainty_aerBsc_raman_532	sr^{-1} m^{-1}	height	Uncertainty of aerosol backscatter coefficient at 532 nm

[End of ESA-L2A+ DI02 - “ASKOS Datasets” - Final Version]